Optics Letters

Supergrowth in speckle patterns

Valeria Viteri-Pflucker,[1,2] Christopher J. Ryan,[1,3] Sethuraj K. R.,[1,2] Kevin Liang,[1,4] David Spiecker,[1] S. A. Wadood,[1,2,5] Andrew N. Jordan,[2,6,7] and A. Nick Vamivakas[1,2,7,*]

[1]The Institute of Optics, University of Rochester, Rochester, New York 14627, USA
[2]Center for Coherence and Quantum Optics, University of Rochester, Rochester, New York 14627, USA
[3]Department of Physics, University of Connecticut, Storrs, Connecticut 06269, USA
[4]Currently with Physics Department, Adelphi University, Garden City, New York 11530, USA
[5]Currently with Department of Electrical and Computer Engineering, Princeton University, New Jersey 08544, USA
[6]Institute for Quantum Studies, Chapman University, Orange, California 92866, USA
[7]Department of Physics and Astronomy, University of Rochester, Rochester, New York 14627, USA
*nick.vamivakas@rochester.edu

Received 6 November 2024; revised 6 December 2024; accepted 9 December 2024; posted 9 December 2024; published 19 December 2024

Supergrowth occurs when the local amplitude growth rate of a wave is greater than that predicted by the band limit. While generating supergrowth on demand requires precise source modulation, we demonstrate that supergrowth occurs naturally in a sum of random plane waves. We measure the supergrowing fractional area of transverse, monochromatic, fully developed speckle patterns. For speckle with a disk spectrum, we find that the average fractional supergrowing area approaches 20%. We compare the supergrowing and superoscillating fractional areas and find great similarity in behavior. Our results inform on the ubiquity of superphenomena in speckle patterns and are relevant to imaging and estimation.

https://doi.org/10.1364/OL.546636

Transverse optical fields are band limited by the optical systems they propagate through. The band limit determines the highest spatial frequency that makes it through the system, and conventionally limits the smallest features of the fields that exit the system [1]. Any band limited wave is said to be superoscillating locally wherever it exhibits oscillations faster than the band limit [2]. The discovery of such waves has led to advances in superresolved imaging and subwavelength focusing [3,4]. There is no theoretical resolution limit because any local behavior can be achieved irrespective of band limit, but at the cost of undesired high-energy regions, making the energy in the superoscillating region relatively small [5]. The high-energy regions make superoscillations challenging to synthesize and measure experimentally. A phenomenon distinct from superoscillations, supergrowth, may be applicable to superresolved imaging with the benefit that supergrowing regions can contain exponentially larger irradiance compared to superoscillatory regions [6].

Supergrowth occurs wherever a band limited wave exhibits growth surpassing the band limit [7]. A reconstructive superresolution imaging modality that uses supergrowing point spread functions has been proposed [6]. In addition, a systematic route to designing supergrowing optical fields with any local behavior has been demonstrated [5]. Supergrowth has also been synthesized experimentally in Ref. [8], which reports the first experimental realization of engineered supergrowing fields.

A natural question to ask is if supergrowth exists naturally, or if it must always require field engineering. Reference [9] has shown that superoscillations can be found in the superposition of isotropic Gaussian random waves, or in speckle patterns. Speckle occurs when coherent light is reflected by or transmitted through optically rough surfaces and is characterized by bright and dark spots caused by interference [10]. Optical speckle has a rich history of applications in coherent imaging [10], interferometry [11], and spectroscopy [12]. In addition, the dark spots in speckle are collections of optical vortices [13] that act as hotspots for superbehavior.

In this work, we experimentally generate speckle patterns with varying power spectra and find that supergrowth can occur over a significant fractional area of a wave. On average, the fractional supergrowing area approaches 20% for speckle with a disk spectrum. To directly compare the nature of supergrowth and superoscillations, we simulate speckle fields and compare the fractional supergrowing and superoscillating areas. We apply the theoretical treatment of the fractional superoscillatory area from Ref. [9] to supergrowth and find that superoscillations and supergrowth should occur at the same rates in random waves.

Mathematical background. In this work, we analyze band limited speckle patterns with a band limit k_{max}. The wave is composed of a superposition of Gaussian random plane waves, resulting in the field $\psi(\boldsymbol{\rho})$ with $\boldsymbol{\rho} = (u, v)$ in the detector plane. Let us define a local wavenumber $k(\boldsymbol{\rho})$ and local growth rate $\kappa(\boldsymbol{\rho})$ such that our scalar field ψ is

superoscillatory, where

$$k = |\mathrm{Im}\{\nabla \log(\psi)\}| > k_{max}, \quad (1)$$

and supergrowing, where

$$\kappa = |\mathrm{Re}\{\nabla \log(\psi)\}| > k_{max}. \quad (2)$$

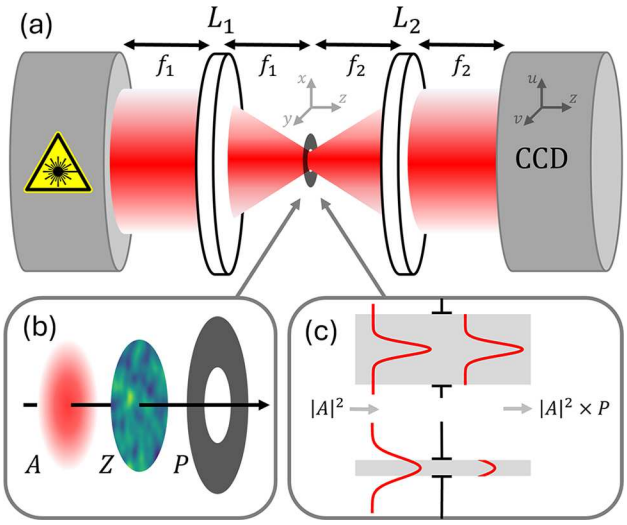

Fig. 1. (a) A $4f$ system is used to generate band limited speckle fields. L_1 and L_2 are lenses with focal lengths of f_1 and f_2, respectively. (b) Elements at the Fourier plane, including the incident Gaussian beam with amplitude A, ground glass with surface height Z, and pinhole with transmittance P. (c) Cross sections of the power spectra most and least resembling a disk spectrum in the experiment. The beam irradiance $|A|^2$ is truncated by the pinhole P, producing an approximate Gaussian spectrum (top, $D = 0.19$) or a disk spectrum (bottom, $D = 0.84$).

Experimentally, we measure the irradiance that has a doubled local growth rate [8]:

$$\nabla \log(\psi^* \psi) = 2\kappa. \tag{3}$$

The irradiance has no phase information, so the local wavenumber cannot be extracted. In the simulation, we have access to the field, so all three definitions are used and a comparison of the local wavenumber and local growth rate can be made.

The fractional supergrowing area f can be predicted using the same formalism as was used in Ref. [9] where we use the local growth rate rather than the local wavenumber:

$$f = \int_{2k_{max}}^{\infty} \frac{4k_2\kappa}{(2k_2 + \kappa^2)^2} d\kappa = \frac{k_2}{k_2 + 2k_{max}^2}, \tag{4}$$

where k_2 is the normalized second moment of the power spectrum. Note that the power spectrum is proportional to the magnitude squared of the angular spectrum of the speckle. Spectrum refers to power spectrum unless otherwise specified. The integrand in Eq. (4) is the probability that a particular growth rate κ will occur in a speckle pattern. The symmetry between superoscillations and supergrowth arises from the fact that this probability is the same for both κ (supergrowth) and k (superoscillation) in Gaussian random waves.

Experiment. To generate speckle patterns with a controllable spectrum, we use a $4f$ optical system with a precision pinhole and ground glass diffuser at the Fourier plane; see Fig. 1(a). The system images a Gaussian beam profile in the front focal plane onto a detector. The pinhole at the Fourier plane is the stop of the system and the ground glass imposes a phase in the stop. Lenses with focal lengths of 300 mm and 500 mm were interchanged for L_1 and L_2 to control the spot size at the Fourier plane. Both lenses have a 1 in. diameter. The system numerical aperture set by the pinhole is smaller than the numerical apertures of both lenses for all system configurations, confirming that the pinhole is the limiting aperture. A 600-grit ground glass diffuser is used (Thorlabs DG10-600). The precision pinholes used have diameters between 40 μm and 150 μm.

The illumination source is a fiber-coupled Fabry–Perot laser operating at a wavelength of 635 nm (Thorlabs S1FC635). The laser light is collimated out of a single-mode fiber using a 15 mm focal length lens. To precisely control the spectrum of the speckle, the illumination needs to be well-known. It was theoretically calculated that the Gaussian beam radius (w_0, the distance from the beam axis where the irradiance drops to $1/e^2$ the maximum value) is between 2.0 mm and 3.4 mm after collimation and was experimentally determined to be 2.19 mm [14]. A Trius Camera SX-814 was used to image the speckle patterns.

To determine the fractional area of a typical speckle pattern that is supergrowing, 100 randomly generated speckle patterns were recorded and their supergrowing fractional areas averaged. We determined that averaging 100 speckle realizations was sufficient using the simulation. A set of random speckle patterns with the same spectrum is created by illuminating a new region of the ground glass by manual rotation of the glass.

To calculate the supergrowing regions of each speckle realization, we first subtract the background from each image. Since a discrete gradient is required, it is highly susceptible to noise. To circumvent the noise, we perform a Gaussian convolution on the image with a convolution kernel smaller than the diffraction-limited spot size at the detector plane. Next, the local growth rate is discretely calculated in accordance with Eq. (3). The resulting supergrowing regions have a tendency to be grouped into smaller sections than in the simulations, which we attribute to the noise in the collection. To group contiguous supergrowing regions, the local growth array is also convolved with a Gaussian kernel. The sum of the FWHMs of the two Gaussian kernels is smaller than the diffraction-limited spot size. The simulation confirms that the convolutions do not affect the supergrowing areas.

Simulation. The speckle recorded by the detector is equivalent to a Fraunhofer propagation of the field at the Fourier plane [1]. To simulate the speckle patterns produced by the experiment, descriptions of the pinhole $P(\mathbf{r})$, the incident beam amplitude $A(\mathbf{r})$, and the ground glass surface height $Z(\mathbf{r})$ are required, where $\mathbf{r} = (x, y)$ is a coordinate at the Fourier plane. The pinhole transmittance $P(\mathbf{r})$ is unity within the clear aperture of the pinhole and zero outside. We approximate the beam amplitude as Gaussian since the fundamental mode of a fiber can be approximated as a Gaussian with 96% accuracy [14]. Letting the Gaussian beam radius be w_o after collimation, at the Fourier plane, the beam radius will be $w_r = \lambda f_1/(\pi w_o)$.

To model $Z(\mathbf{r})$, we need to generate statistically accurate, random instances of the ground glass surface used. The simulated ground glass surfaces match the experimentally collected values for the surface profile arithmetical mean deviation R_a, the surface profile root mean square deviation R_q, and the transverse correlation length l_c. The values for R_a (1.483 μm) and R_q (1.939 μm) were measured using a contact-type surface roughness measurement instrument in Ref. [15]. A correlation length of 30 μm was found to mimic the experimentally collected surface profiles. We match R_a, R_q, and l_c by generating an array of random numbers, convolving it with a Gaussian with the FWHM of l_c, scaling to match R_q, and raising the array by the power of 1.14 to match R_a. An example simulated ground glass surface profile is depicted in Fig. 1(b) labeled as Z, where the diameter of the ground

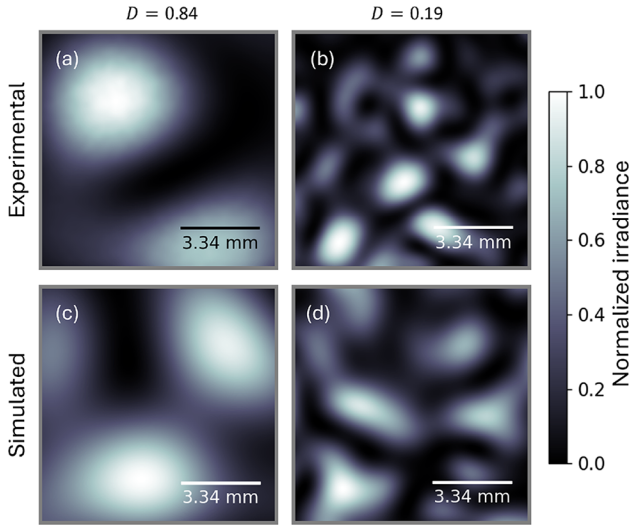

Fig. 2. Example simulated and experimental speckle patterns for lens focal lengths $f_1 = 500$ mm and $f_2 = 300$ mm with pinhole radii of 20 μm in (a) and (c) and 75 μm in (b) and (d). The simulation produces speckle patterns with similar feature sizes as the experiment.

glass section shown is 150 μm. We found that for all pinhole sizes used, the speckle produced approximately obeys Gaussian statistics.

With each element at the Fourier plane accurately modeled, we can perform a discrete Fraunhofer propagation to find the field at the detector U_d, ignoring a constant amplitude term:

$$U_d(\boldsymbol{\rho}) = \iint A(\mathbf{r})P(\mathbf{r}) \exp\left[i\frac{2\pi}{\lambda}\left(Z(\mathbf{r}) - \frac{\mathbf{r}\cdot\boldsymbol{\rho}}{f_2}\right)\right] d^2\mathbf{r}. \quad (5)$$

It was found that the sampling at Nyquist produced speckle with experimentally accurate feature sizes, but smaller superbehaved fractional areas than theoretically predicted [9]. Consequently, we sample at double the Nyquist rate. Examples of experimental and simulated speckle patterns are shown in Fig. 2. It is evident that the feature sizes in the simulation and experiment agree.

In our experiment, the spectrum is a clipped Gaussian that behaves more Gaussian or more disk-like depending on the pinhole and lens combination used. To quantify how close to a disk spectrum a particular system configuration's power spectrum is, we define the following overlap integral:

$$D = \frac{\iint A(\mathbf{r})A^*(\mathbf{r})P(\mathbf{r})d^2\mathbf{r}}{A(0)A^*(0)\pi r_{pin}^2}. \quad (6)$$

If the incident beam is a uniform plane wave ($A(\mathbf{r})$ constant), the spectrum is a perfect disk spectrum after passing through the pinhole, and the overlap integral has a value of unity. If the incident beam is Gaussian with a small beam waist relative to the pinhole, the overlap integral approaches zero. The cross sections of the spectra with the highest (0.84) and lowest (0.07) overlap integral values are plotted in Fig. 1(c). The supergrowing behavior of speckle patterns has not been explored, so we experimentally, computationally, and theoretically investigate the supergrowing behavior of speckle patterns as the spectrum changes.

Results. The local wavenumber and local growth rate are calculated from a simulated speckle pattern using a discrete

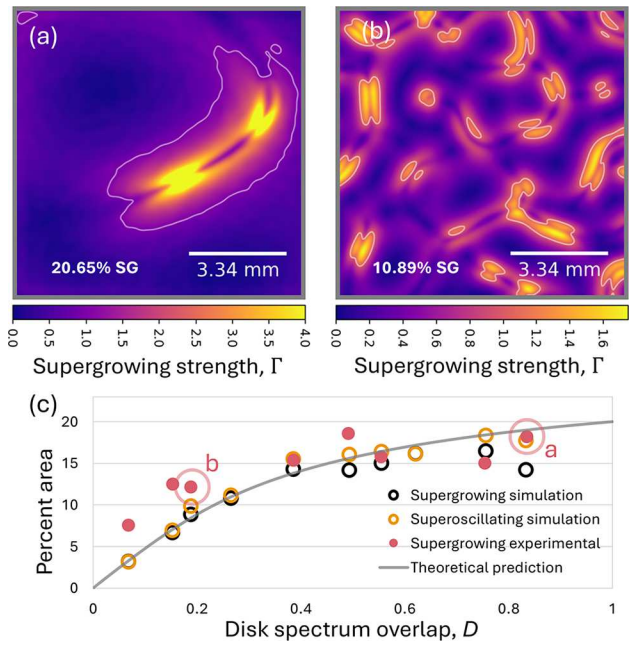

Fig. 3. (a) and (b) Local supergrowing strength $\Gamma = |\kappa/k_{max}|$ for the speckle patterns in Figs. 2(a) and 2(b). The white contours enclose supergrowing regions. These speckle patterns were chosen because their fractional supergrowing areas are similar to the average for their spectral shape. (c) Average fractional supergrowing or superoscillating area for different spectral shapes, quantified by the disk spectrum overlap integral D. Each data point is averaged from 100 speckle realizations. The circled data points correspond to the data sets (a) and (b) to which they belong. The gray curve shows the theoretical prediction for the superbehaved fractional area.

gradient as in Eqs. (1) and (2). The local growth rate is determined from an experimentally collected speckle pattern using Eq. (3). The local growth rates of the experimental speckle patterns in Figs. 2(a) and 2(b) are depicted in Figs. 3(a) and 3(b). The color bars are quantified by $\Gamma = |\kappa/k_{max}|$, the supergrowing strength [8]. When Γ is greater than unity, the speckle pattern is locally supergrowing. White contours enclose such supergrowing regions. We note that for Fig. 3(a), the color bar value is intentionally thresholded at 64% of the speckle pattern's maximum supergrowing strength for better visualization of the local growth behavior. It has been well documented that superoscillations occur in low irradiance regions of fields, and it has been theoretically demonstrated that the fractional energy in a superoscillating/supergrowing region is limited by the size of the region and the local rates of oscillation/growth [3,5]. As such, the supergrowing regions in Figs. 3(a) and 3(b) are in the low irradiance regions of Figs. 2(a) and 2(b). The supergrowth and superoscillations tend to overlap but are not identical in the simulation.

Figure 3(c) contains the results of averaging the supergrowing and superoscillating fractional areas of 100 speckle realizations for varying spectrum shapes. We also find the predicted fractional superbehaved area using Eq. (4). Knowing the power spectrum of the speckle patterns to be a scaled version of the irradiance at the Fourier plane, the normalized second moment of the power spectrum can be calculated as

follows:

$$k_2 = \frac{\int_0^{2\pi}\int_0^{k_{max}} k_r^2 e^{-2k_r^2/w_k^2} k_r dk_r d\theta}{\int_0^{2\pi}\int_0^{k_{max}} e^{-2k_r^2/w_k^2} k_r dk_r d\theta} = \frac{w_k^2}{2} - \frac{k_{max}^2}{e^{2k_{max}^2/w_k^2} - 1}, \quad (7)$$

where $k_r = 2\pi r/(\lambda f_2)$ is a spatial frequency, θ is an angle in the Fourier plane, $w_k = 2f_1/(w_0 f_2)$ is the beam radius in k-space, and $k_{max} = 2\pi r_{pin}/(\lambda f_2)$. If A was constant, then our speckle would have a disk spectrum and $k_2 = k_{max}^2/2$, which results in the fractional supergrowing and superoscillating areas being 20%. Substituting Eq. (7) into Eq. (4) for all values of D returns the gray prediction curve in Fig. 3(c).

The superoscillating and supergrowing fractional areas in the experiment and the simulation have the same behavior as the theoretical curve. The fractional areas approach 20% as D approaches unity and diminish as D approaches zero. The reason for the latter is as D goes to zero, the spectrum becomes more Gaussian, implying that the highest spatial frequencies allowed through the system have low relative amplitudes compared to the lower spatial frequencies as is shown in Fig. 1(c). As a result, the field resembles a field with a smaller band limit (speckle blobs are large) but with a higher value of k_{max}, making it hard to locally achieve superoscillations. The supergrowing and superoscillating regions of the fields tend to occur near phase vortices in the speckle pattern, causing large overlap regions and subsequently similar average fractional superbehaved areas. We find that supergrowth and superoscillations occur at the same rates in random waves. For the experimental data set with the highest overlap integral value, $D = 0.84$, the average fractional supergrowing area is 18.18% with a standard deviation of 7.28%. The peak supergrowing fractional area of this data set is 41.8%, so individual speckle realizations can have higher supergrowing areas. Overall, a significant fractional area of a wave can be supergrowing.

For lower D values, the experimental fractional supergrowing areas are higher than the theoretical curve. Lower D values imply larger pinhole sizes, which create smaller speckle patterns. Upon comparing Figs. 3(a) and 3(b), it is evident that the total perimeter of the contours is larger for the case with smaller speckle patterns. The borders of the supergrowing regions are susceptible to noise, which causes higher supergrowing regions to be detected for smaller values of D. We also see the least agreement between the simulation and the theoretical curve for the highest D value, 0.84. For large D values, the decreased pinhole size causes the speckle to deviate from Gaussian statistics. The smallest pinhole used has a diameter of 40 μm because this is a cutoff for generating fully developed speckle for the ground glass used. Simulated speckle patterns using smaller pinholes were not fully developed and were not accurately predicted by the theoretical curve. As long as the phase imparted by the ground glass is random, the particular glass surface profile features do not affect the final supergrowth statistics.

Concluding remarks. In summary, we experimentally synthesized band limited speckle patterns with varying spectra to explore the average fractional supergrowing area of random Gaussian waves. The speckle patterns were created by using a 4f optical system with ground glass and a precision pinhole at the Fourier plane, illuminated by a Gaussian beam. Eight different power spectra were generated by using different combinations of lenses and pinholes. We compared experimental and theoretical results to a simulation in order to bridge superoscillations and supergrowth in speckle patterns without measuring the full field of the experimentally recorded speckle patterns. The simulation modeled the experiment, particularly by modeling the optically rough ground glass surface. To find the average superbehaved fractional area for a given spectrum, 100 or more speckle patterns were recorded or simulated and their individual superbehaved fractional areas averaged.

Our results have potential biophotonic applications utilizing speckle statistics. Laser speckle contrast analysis is a technique that utilizes the spatial variations of speckle patterns to determine capillary blood flow [16]. Supergrowth calculations are also dependent on the spatial variations of speckle patterns and may have the capacity to yield similar information.

Superoscillations are already a rich area of research for superresolution modalities, and supergrowth holds promise for opening new avenues in superresolution research. Our results suggest that supergrowth, like superoscillation, is intrinsic to speckle patterns and that it can occur in high fractional areas of fields. Our results provide support for the viability of supergrowth in superresolution imaging, parameter estimation, and ranging [6,7,17]. Speckle occurs ubiquitously in optics, so this investigation of its fundamental physics sheds new light on the robustness of supergrowth in the natural world.

Funding. Air Force Office of Scientific Research (FA9550-21-1-0322, FA9550-24-1-0329); Bill Hannon Foundation.

Acknowledgment. Valeria Viteri-Pflucker thanks Anis Idrizović for assistance in quantifying ground glass properties, Mathew McClure for discussions on background management in experimental speckle data, and Tathagata Karmakar for helpful discussions on supergrowth.

Disclosures. The authors declare no conflicts of interest.

Data availability. Data underlying the results presented in this paper are not publicly available at this time but may be obtained from the authors upon reasonable request.

REFERENCES

1. J. W. Goodman, *Introduction to Fourier Optics*, 4th ed. (W. H. Freeman and Company, 2017).
2. M. Berry, N. Zheludev, Y. Aharonov, *et al.*, J. Opt. **21**, 053002 (2019).
3. G. Gbur, Nanophotonics **8**, 205 (2019).
4. G. Chen, Z.-Q. Wen, and C.-W. Qiu, Light: Sci. Appl. **8**, 56 (2019).
5. T. Karmakar and A. N. Jordan, J. Phys. A: Math. Theor. **56**, 495204 (2023).
6. T. Karmakar, A. Chakraborty, A. N. Vamivakas, *et al.*, Opt. Express **31**, 37174 (2023).
7. A. N. Jordan, Quantum Studies: Math. Found. **7**, 285 (2020).
8. K. R. Sethuraj, T. Karmakar, S. A. Wadood, *et al.*, Phys. Rev. Res. **6**, L032043 (2024).
9. M. R. Dennis, A. C. Hamilton, and J. Courtial, Opt. Lett. **33**, 2976 (2008).
10. J. W. Goodman, *Speckle Phenomena in Optics: Theory and Applications* (Ben Roberts, 2007).
11. K. Creath, Appl. Opt. **24**, 3053 (1985).
12. H. Cao, J. Opt. **19**, 060402 (2017).
13. G. J. Gbur, *Singular Optics* (CRC Press, 2017).
14. C. R. Pollock and M. Lipson, *Integrated Photonics* (Springer, 2003).
15. D. Wei, T. Katagiri, and M. Aketagawa, in *Optical Metrology and Inspection for Industrial Applications IV* (SPIE, 2016), p. 100231M.
16. J. D. Briers and S. Webster, J. Biomed. Opt. **1**, 174 (1996).
17. J. C. Howell, A. N. Jordan, B. Šoda, *et al.*, Phys. Rev. Lett. **131**, 053803 (2023).